Dynamical density and spin response functions of two-dimensional correlated fermion systems: Self-consistent second-order perturbation theory

A. Kotani[1] and D. S. Hirashima[1,2]

[1]*Department of Physics, Nagoya University, Nagoya 464-8602, Japan*

[2]*Department of Material Science, International Christian University, Mitaka, Tokyo 180-8585, Japan*

(Received 18 March 2013; revised manuscript received 27 June 2013; published 30 July 2013)

Dynamical density and spin responses of a two-dimensional fermion system are studied with the self-consistent second-order perturbation theory using a model Hamiltonian. Special attention is paid to the density response at a large wave vector, where it was reported that a sharp mode develops below the particle-hole continuum in two-dimensional liquid ^{3}He. We find that at a large wave vector, a peak in the dynamical density structure factor shifts to lower energy as interaction sets in, but it is not sharp enough to represent a well-defined mode because of the strong damping effect of the quasiparticles. We point out that it is necessary to treat the large damping effect properly in explaining the propagating mode found in two-dimensional liquid ^{3}He.

DOI: 10.1103/PhysRevB.88.014529 PACS number(s): 67.30.em, 67.30.ej

I. INTRODUCTION

Recently, Godfrin *et al.*[1,2] performed an inelastic neutron scattering experiment on monolayer liquid ^{3}He adsorbed on graphite. They succeeded in observing the particle-hole (p-h) continuum spectrum characterizing the Fermi liquid state of two-dimensional (2D) liquid ^{3}He. At a small wave vector, $q = k_F$, where k_F is the Fermi wave vector, they found that the spectrum has a peak at a frequency higher than the p-h continuum threshold. They ascribed it to the zero sound mode. The zero sound mode was found to enter the p-h band at an intermediate wave vector. At a larger wave vector, $q \simeq 3k_F$, a sharp peak in the spectrum was found *below* the p-h band. This implied that the zero sound mode reappeared outside the p-h band at a large wave vector. Then, the dispersion relation of the zero sound mode could be very similar to the phonon-roton dispersion curve in superfluid ^{4}He. A theoretical analysis was also given in Refs. 1 and 2, supporting this interpretation. At present, it appears that this interpretation works satisfactorily, but these experimental findings warrant more studies with various approaches.

The purpose of this study is to calculate the dynamical response functions of a 2D interacting fermion system and find the possible collective mode dispersion. It is well known that the low-energy and long-wavelength dynamics of bulk liquid ^{3}He is well described with the Landau Fermi liquid theory. The Landau Fermi liquid theory is also applicable to 2D fermion systems if the lattice effect is negligible. The zero sound mode at a small wave vector is indeed well explained with the Fermi liquid theory (or its extension). However, dynamics at large wave vectors and high energies is not necessarily described with the phenomenological Fermi liquid theory. In this paper, starting from a model Hamiltonian, we study the dynamics of a 2D interacting fermion system microscopically.

The most conventional microscopic approach to the study of dynamical responses is the random phase approximation (RPA) combined with the effective interaction potential. The effective potential can be obtained phenomenologically.[3,4] A model with frequency- and wave-vector-dependent effective mass has also been used in the calculation of dynamical responses of liquid ^{3}He.[5] These approaches are essentially an extension of the Landau Fermi liquid theory, and the applicability to high-energy and short-wavelength dynamics is questionable.

Extension of the simple RPA has been an important subject. Dynamical correlations beyond the RPA, that is, pair fluctuations, have been considered with the correlated-basis-functions (CBF) theory, and the effective interaction and the dynamic structure factor were calculated with this approach.[6–8] Theoretical interpretation presented in Refs. 1 and 2 was based on this theory, where the exchange effect, which is often neglected in the RPA, was not fully considered, either. On the other hand, when the exchange effect is considered, pair fluctuations are neglected.[9] Recently, the theory has been extended with the inclusion of the exchange effects in addition to the dynamic self-energy corrections.[10]

Another microscopic approach is the T-matrix theory. It has indeed been elaborately applied to bulk liquid ^{3}He, and the effective interaction and dynamical response functions were calculated.[11–14] In this approach, full self-consistency between the single-particle Green's function and the self-energy has not been achieved. For example, the self-consistency is achieved only for on-shell self-energy.[11–14] A fully self-consistent calculation would be a numerically formidable task at present. The T-matrix theory was also applied to 2D ^{3}He, but it is not a self-consistent calculation, either, and far from complete.[15] Thus, study of dynamical responses in liquid ^{3}He beyond the RPA has much room for improvement now.

In this paper, we take a semi-phenomenological approach and start from model interaction potential with a soft core. The model potential is chosen quite arbitrarily, and we can draw only qualitative conclusions from this study. However, we study the correlation effect systematically and self-consistently. The interaction potential is treated with the self-consistent second-order perturbation theory (SCSOPT) and the self-energy effect is self-consistently considered. Here, not only the real part but also the imaginary part of the self-energy (the damping rate) are calculated. Moreover, the vertex corrections for dynamical response functions are also considered as correctly as possible so that the sum rules are satisfied. Moreover, in the calculation, the exchange terms are fully considered. Thus, the present calculation includes the

effect of the correlation and the exchange processes, although the direct quantitative relevance to real ^{3}He is limited.

First, with the RPA,[16] we study the effect of the exchange terms and point out the importance of the spatial dependence of the interaction potential $V(r)$. Suppose that the Hamiltonian of an interacting spin-1/2 fermion system is given as

$$\mathcal{H} = \sum_{\boldsymbol{k},\sigma} \epsilon_k c^\dagger_{\boldsymbol{k},\sigma} c_{\boldsymbol{k},\sigma} + \frac{1}{2}\sum_{\boldsymbol{q}} V(q) \times \sum_{\boldsymbol{k},\boldsymbol{k}',\sigma\sigma'} c^\dagger_{\boldsymbol{k}+\boldsymbol{q},\sigma} c^\dagger_{\boldsymbol{k}'-\boldsymbol{q},\sigma'} c_{\boldsymbol{k}',\sigma'} c_{\boldsymbol{k},\sigma}, \tag{1}$$

where $c_{\boldsymbol{k},\sigma}$ ($c^\dagger_{\boldsymbol{k},\sigma}$) is an annihilation (creation) operator of a fermion of momentum $\boldsymbol{k}$ and spin σ, ϵ_k is the kinetic energy, and $V(q)$ is the Fourier transform of the model potential $V(r)$, which is assumed to be short ranged and dominantly repulsive. We are concerned with dynamical density and spin response functions. The dynamical density susceptibility $\chi_c(\boldsymbol{q},\omega+i\delta)$ is defined by

$$\chi_c(\boldsymbol{q},\omega+i\delta) = \frac{i}{N}\int_0^\infty dt e^{i(\omega+i\delta)t} \sum_{\sigma,\sigma'} \langle [n_\sigma(\boldsymbol{q},t), n_{\sigma'}(-\boldsymbol{q},0)]\rangle, \tag{2}$$

where N is the fermion number, the square bracket is the commutator, and

$$n_\sigma(\boldsymbol{q}) = \sum_{\boldsymbol{k}} c^\dagger_{\boldsymbol{k},\sigma} c_{\boldsymbol{k}+\boldsymbol{q},\sigma}. \tag{3}$$

The dynamical spin susceptibility $\chi_s(\boldsymbol{q},\omega+i\delta)$ is defined by

$$\chi_s(\boldsymbol{q},\omega+i\delta) = \frac{i}{N}\int_0^\infty dt e^{i(\omega+i\delta)t} \times \sum_{\sigma,\sigma'} \sigma\sigma' \langle [n_\sigma(\boldsymbol{q},t), n_{\sigma'}(-\boldsymbol{q},0)]\rangle. \tag{4}$$

In the RPA, we can readily calculate the dynamical susceptibilities if the exchange terms are neglected,

$$\chi_c(\boldsymbol{q},\omega+i\delta) = \frac{2P_0^{(0)}(\boldsymbol{q},\omega+i\delta)}{1+2V(q)P_0^{(0)}(\boldsymbol{q},\omega+i\delta)} \tag{5}$$

and

$$\chi_s(\boldsymbol{q},\omega+i\delta) = 2P_0^0(\boldsymbol{q},\omega+i\delta), \tag{6}$$

where $P_0^{(0)}(\boldsymbol{q},\omega+i\delta)$ is the Lindhard function,

$$P_0^{(0)}(\boldsymbol{q},z) = \frac{1}{N}\sum_{\boldsymbol{k}} \frac{f(\xi_k)-f(\xi_{k+q})}{z+\xi_{k+q}-\xi_k}, \tag{7}$$

where $\xi_k = \epsilon_k - \mu$ with μ being the chemical potential and $f(x)$ is the Fermi distribution function. Without the spin dependence of the interaction potential, the spin susceptibility is unchanged by the interaction in this approximation. In the long-wavelength region, $q \ll k_F$, $\mathrm{Re}P_0^{(0)}(q,\omega) < 0$ for $\omega > v_F q$ and logarithmically diverges as $q \to 0$ with a fixed value of $\omega/v_F q$, where v_F is the Fermi velocity. This divergence necessarily gives rise to the zero sound mode in the $q \to 0$ limit for $V(q=0) > 0$. On the other hand, in the short-wavelength region, $q > 2k_F$, $\mathrm{Re}P_0^{(0)}(q,\omega) > 0$ at $\omega < v_F(q-2k_F)$, that is, below the p-h band. If $V(q)$ remains positive at $q > 2k_F$, no collective mode appears in the density channel in the short-wavelength region. For a density collective mode to appear below the p-h band without the exchange processes, $V(q)$ must be negative at $q \gtrsim 2k_F$.

In the presence of the exchange processes, the dynamical susceptibilities cannot be calculated in a closed form. To obtain qualitative understanding, we make a further approximation. To consider only interaction between fermions around the Fermi surface in 2D, we approximate the interaction $V(\boldsymbol{k}-\boldsymbol{k}')$ as

$$V(\boldsymbol{k}-\boldsymbol{k}') \simeq V(\boldsymbol{k}_F - \boldsymbol{k}'_F) = V\left(\cos\left(\theta_{\boldsymbol{k}_F} - \theta_{\boldsymbol{k}'_F}\right)\right) = v_0 + \sum_{m\neq 0} v_m \left(\cos m\theta_{\boldsymbol{k}_F}\cos m\theta_{\boldsymbol{k}'_F} + \sin m\theta_{\boldsymbol{k}_F}\sin m\theta_{\boldsymbol{k}'_F}\right), \tag{8}$$

where $\theta_{\boldsymbol{k}}$ is the angle of $\boldsymbol{k}$ measured from the x axis, $v_0 = \int_0^{2\pi} d\theta V(\cos\theta)/(2\pi) = \langle\langle V\rangle\rangle$, etc. Neglecting v_m ($m \neq 0$), we obtain

$$\chi_c(\boldsymbol{q},\omega+i\delta) = \frac{2P_0^{(0)}(\boldsymbol{q},\omega+i\delta)}{1+[2V(q)-\langle\langle V\rangle\rangle]P_0^{(0)}(\boldsymbol{q},\omega+i\delta)} \tag{9}$$

and

$$\chi_s(\boldsymbol{q},\omega+i\delta) = \frac{2P_0^0(\boldsymbol{q},\omega+i\delta)}{1-\langle\langle V\rangle\rangle P_0^{(0)}(\boldsymbol{q},\omega+i\delta)}. \tag{10}$$

It is natural to assume that $V(q)$ is a decreasing function of q. Therefore, $V(q) > \langle\langle V\rangle\rangle > 0$ at $q \ll k_F$, but $V(q)$ can be smaller than $\langle\langle V\rangle\rangle$ for larger q. It is then possible that $2V(q) - \langle\langle V\rangle\rangle < 0$ for larger q even if $V(q) > 0$, and a density collective mode can appear in the short-wavelength region as was suggested in Refs. 1 and 2. At the same time, we can see that the exchange terms can cause the enhancement of the dynamical spin susceptibility. We thus see that the exchange terms have important effects on the dynamical density and spin responses and that the dynamical density response can be significantly affected by the q dependence of $V(q)$.

Although we can obtain some qualitative understanding of the dynamical responses using the RPA, it is far from satisfactory. Indeed, the results obtained with the RPA were found to disagree with experimental results.[7,8] In this study, we study the qualitative changes in the dynamical response functions caused by the correlation effect beyond the RPA. The finite range of interaction potential and the exchange processes must also be important as in the RPA.

In the next section, we introduce a model system of interacting 2D fermions and give a formulation for the calculation of dynamical responses. In Sec. III, we present numerical results, and the last section is devoted to summary and discussion. Some technicalities are detailed in the Appendix. A short account of the present study was published in Ref. 17.

II. MODEL AND THEORY

It is easier to perform a self-consistent perturbation calculation using a lattice model than using a continuous model. To avoid the lattice effect, it is necessary to consider the dilute limit. We thus consider a dilute Hubbard-type model on a square lattice whose lattice constant is a. If one discussed, for example, the solid-liquid transition of 2D

^{3}He, a triangular lattice would be more appropriate. However, the lattice structure does not matter for the present purpose. In addition to the on-site repulsive interaction, we consider repulsive interaction between fermions at different sites,

$$\mathcal{H} = \sum_{\boldsymbol{k},\sigma} \epsilon_k c^\dagger_{\boldsymbol{k},\sigma} c_{\boldsymbol{k},\sigma} + U \sum_i n_{i\uparrow} n_{i\downarrow} + \sum_n \sum_{(i,j)_n} V^{(n)} n_i n_j, \tag{11}$$

where

$$\epsilon_k = -2t(\cos k_x a + \cos k_y a), \tag{12}$$

$$n_i = \sum_\sigma n_{i\sigma} = \sum_\sigma c^\dagger_{i,\sigma} c_{i,\sigma}, \tag{13}$$

and $(i,j)_n$ stands for the nth neighbor pairs. For simplicity, we put $V^{(1)} = V^{(2)} = V_1$ and $V^{(3)} = V^{(4)} = V_2$. Then, the Fourier transform of the potential V_n can be written as

$$\begin{aligned} V(q) = {} & 2V_1[\cos k_x a + \cos k_y a \\ & + \cos(k_x + k_y)a + \cos(k_x - k_y)a] \\ & + 2V_2[\cos 2k_x a + \cos 2k_y a \\ & + \cos(2k_x + k_y)a + \cos(2k_x - k_y)a \\ & + \cos(k_x + 2k_y)a + \cos(k_x - 2k_y)a]. \end{aligned} \tag{14}$$

To avoid the lattice effect, we consider the dilute limit, $n \simeq 0.112$, where n is the total fermion number per lattice point. In this case, the Fermi surface is almost circular and the Fermi wave vector is given by

$$k_F a \simeq \frac{3\sqrt{2}\pi}{16} = 0.265\pi. \tag{15}$$

The bare Fermi energy $\epsilon_F^{(0)}$ is given as

$$\epsilon_F^{(0)} = \epsilon_{k_F} + 4t \simeq 0.674t. \tag{16}$$

In this study, we show numerical results at $T = 0.04t$ unless otherwise stated, and

$$T \simeq 0.06\epsilon_F^{(0)}. \tag{17}$$

To proceed beyond the RPA, we use the second-order perturbation theory. In addition to the Hartree $\Sigma_\sigma^{(H)}$ and Fock terms $\Sigma_\sigma^{(F)}(\boldsymbol{k})$, we consider the second-order self-energy term $\Sigma_\sigma^{(2)}(k)$ shown in Fig. 1. We use the imaginary-time formalism and k is the abbreviation for $(\boldsymbol{k}, i\epsilon_n)$, where ϵ_n is a fermionic Matsubara frequency. Using the self-energy $\Sigma_\sigma(k) = \Sigma_\sigma^{(H)} + \Sigma_\sigma^{(F)}(\boldsymbol{k}) + \Sigma_\sigma^{(2)}(k)$, the single-particle Green's function $G_\sigma(k)$ is expressed as

$$G_\sigma(k) = [i\epsilon_n - \xi_k - \Sigma_\sigma(k)]^{-1}. \tag{18}$$

The self-energy $\Sigma_\sigma(k)$ is also expressed in terms of $G_\sigma(k)$ and has to be self-consistently determined. This is the

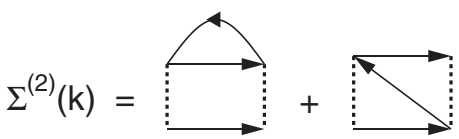

FIG. 1. Diagrams for the second-order self-energy $\Sigma^{(2)}(k)$. Solid lines represent the single-particle Green's function $G(k)$ and dotted lines the interaction [U or $V(\boldsymbol{q})$].

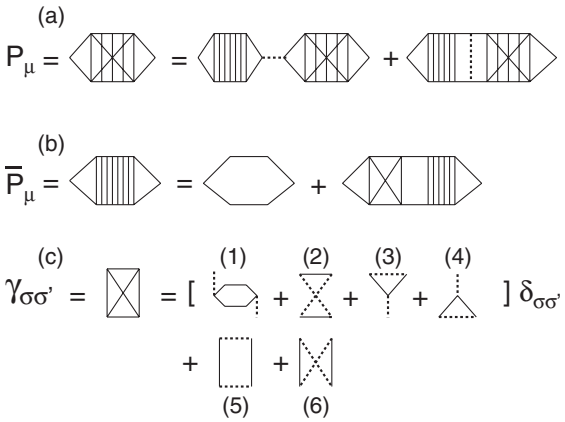

FIG. 2. (a) Polarization function $P_\mu(q)$ [$=\chi_\mu(q)/2$] in terms of irreducible polarization function $\overline{P}_\mu(q)$. (b) Irreducible polarization function $\overline{P}_\mu(q)$ in terms of the p-h irreducible vertex $\gamma_\mu(k,k';q)$. (c) p-h irreducible vertex $\gamma_{\sigma\sigma'}(k,k';q)$ in the second-order perturbation theory. Solid lines represent the single-particle Green's function $G_\sigma(k)$ and dotted lines the interaction [U or $V(\boldsymbol{q})$].

self-consistent second-order perturbation theory (SCSOPT). Explicit expression of $\Sigma^{(2)}(k)$ is given in the Appendix. Once the single-particle Green's function is calculated, we can compute dynamical response functions. In the computation, we have to consider the vertex corrections corresponding to the self-energy so that the resultant dynamical response functions satisfy the conservation laws, for example, the f-sum rule. Diagrammatic expressions for the dynamical density and spin susceptibilities, $\chi_c(q)$ and $\chi_s(q)$, are given in Fig. 2.

Figure 2(b) represents an integral equation for the full 4-point vertex function $\Gamma_\mu(k,k';q)$ or equivalently the 3-point vertex function $\Lambda_\mu(k;q)$ [see Eqs. (A12)–(A16)]. Unfortunately, in the presence of $V(\boldsymbol{q})$, this integral equation is extremely difficult to solve, because the equation is not a convolution equation. If it were a convolution equation, we could efficiently solve it using the fast Fourier transformation (FFT). To be able to apply the FFT, we have to make approximations to the integral equation. First, we neglect (3) and (4) in Fig. 2(c), and then apply a "local" approximation to diagrams (2), (5), and (6). For example, diagram (5) is expressed with the following integral,

$$\sum_{k''} [U + V(\boldsymbol{k}'' + \boldsymbol{q})][U + V(\boldsymbol{k}'')] G(k - k'') G(k' - k''), \tag{19}$$

where (and in the following) spin indices are neglected. We cannot use the FFT for this integral. Then we approximate it by averaging the interaction potential,

$$\begin{aligned} & [U + V(\boldsymbol{k}'' + \boldsymbol{q})][U + V(\boldsymbol{k}'')] \\ & \to \frac{1}{N_L} \sum_{\boldsymbol{k}''} [U + V(\boldsymbol{k}'' + \boldsymbol{q})][U + V(\boldsymbol{k}'')] \\ & = U^2 + W(\boldsymbol{q}), \end{aligned} \tag{20}$$

where

$$W(\boldsymbol{q}) = \frac{1}{N_L} \sum_{\boldsymbol{k}} V(\boldsymbol{k} + \boldsymbol{q}) V(\boldsymbol{k}), \tag{21}$$

with $N_{\rm L}$ being the total number of lattice points. We can then apply the FFT to diagram (5). Further details are explained in the Appendix. The resultant approximate integral equations for the three-point vertex functions are

$$\Lambda_\mu(k;q) = 1 + \sum_{k'} \gamma_\mu(k,k';q) G(k'+q) G(k') \Lambda_\mu(k';q), \tag{22}$$

where

$$\begin{aligned}\gamma_{\rm c}(k,k';q) \simeq\ & [2U^2 + 2UV(\boldsymbol{k}-\boldsymbol{k}') + V(\boldsymbol{k}-\boldsymbol{k}')^2 \\ & + 2W(\boldsymbol{q})] P_0(k-k') - [U^2 + 2W(\boldsymbol{q})] \\ & \times K_0(k+k'+q) + \gamma^{(2)}(q'),\end{aligned} \tag{23}$$

and

$$\begin{aligned}\gamma_{\rm s}(k,k';q) \simeq\ & [2UV(\boldsymbol{k}-\boldsymbol{k}') + V(\boldsymbol{k}-\boldsymbol{k}')^2] P_0(k-k') \\ & + U^2 K_0(k+k'+q) + \gamma^{(2)}(q'),\end{aligned} \tag{24}$$

where

$$P_0(q) = -\sum_k G(k+q) G(k), \tag{25}$$

$$K_0(K) = \sum_k G(K+k) G(-k), \tag{26}$$

$$\gamma^{(2)}(q') = \sum_r e^{-iq'r} \sum_J V^{(n)2} G(r) G(r) \delta_{\boldsymbol{r},\boldsymbol{\delta}_J}, \tag{27}$$

$q = (\boldsymbol{q}, i\omega_m)$, $q' = (\boldsymbol{q}, i(\epsilon_n + \epsilon_{n'} + \omega_m))$, and $\sum_k = (1/N_{\rm L}) \sum_{\boldsymbol{k}} T \sum_n$. See also the Appendix for the definitions of J and $\boldsymbol{\delta}_J$. A more detailed description of the procedure to calculate dynamical response functions is given in the Appendix.

Here, we should note that, in the presence of the vertex corrections, the irreducible polarization function $\overline{P}_\mu(q)$ can be expressed as

$$\overline{P}_\mu(q) = P_0(q) + \Delta P_\mu(q). \tag{28}$$

Neglecting the exchange processes, the dynamical density susceptibility is expressed by

$$P_{\rm c}(q) = \frac{P_0(q) + \Delta P_{\rm c}(q)}{1 + [U + 2V(\boldsymbol{q})][P_0(q) + \Delta P_{\rm c}(q)]}. \tag{29}$$

We can then rewrite the denominator as

$$1 + \tilde{V}_{\rm c}(q) P_0(q), \tag{30}$$

where

$$\tilde{V}_{\rm c}(q) = [U + 2V(\boldsymbol{q})] \left[1 + \frac{\Delta P_{\rm c}(q)}{P_0(q)} \right]; \tag{31}$$

that is, the vertex correction is partly equivalent to the introduction of energy-dependent complex effective interaction $\tilde{V}_\mu(q)$.

We assess the validity of the approximations for irreducible vertices with two methods. We introduce the dynamical structure factors $C(\boldsymbol{q},\omega)$ and $S(\boldsymbol{q},\omega)$,

$$C(\boldsymbol{q},\omega) = \int_{-\infty}^{\infty} \frac{dt}{2\pi N} e^{i\omega t} \sum_{\sigma,\sigma'} \langle \Delta n_\sigma(\boldsymbol{q},t) \Delta n_{\sigma'}(-\boldsymbol{q},0) \rangle, \tag{32}$$

where $\Delta n_\sigma(\boldsymbol{q},t) = n_\sigma(\boldsymbol{q},t) - \langle n_\sigma(\boldsymbol{q},t) \rangle$, and

$$S(\boldsymbol{q},\omega) = \int_{-\infty}^{\infty} \frac{dt}{2\pi N} e^{i\omega t} \sum_{\sigma,\sigma'} \sigma\sigma' \langle n_\sigma(\boldsymbol{q},t) n_{\sigma'}(-\boldsymbol{q},0) \rangle. \tag{33}$$

They are related to dynamical susceptibilities through the fluctuation-dissipation theorem,

$$M(\boldsymbol{q},\omega) = \frac{1}{\pi} [1 + f_{\rm B}(\omega)] {\rm Im} \chi_\mu(\boldsymbol{q}, \omega + i\delta) \quad (M,\mu = C,S), \tag{34}$$

where $f_{\rm B}(x)$ is the Bose distribution function, $f_{\rm B}(x) = 1/(e^{\beta x} - 1)$. It is well known that response functions in the imaginary-time representation are expressed in terms of the dynamical structure factors as

$$\chi_\mu(\boldsymbol{q},\tau) = \int_{-\infty}^{\infty} d\omega e^{-\tau\omega} M(\boldsymbol{q},\omega) \quad (M,\mu = C,S). \tag{35}$$

From this, we can derive the compressibility sum rule,

$$\begin{aligned}\chi_{\rm c} = \chi_{\rm c}(\boldsymbol{q} \to 0, i\omega = 0) &= \int_0^\beta d\tau \chi_{\rm c}(\boldsymbol{q} \to 0, \tau) \\ &= 2 \int_{-\infty}^{\infty} \frac{d\omega}{\omega} C(\boldsymbol{q} \to 0, \omega).\end{aligned} \tag{36}$$

We can also obtain a similar relation for the spin susceptibility. We can then use the compressibility sum rule to check the validity of the approximation. The compressibility $\chi_{\rm c}$ can be calculated by solving the self-consistent equation for two slightly different values of the chemical potential μ, $\chi_{\rm c} = \partial n/\partial\mu$. By comparing this and $\chi_{\rm c}(\boldsymbol{q} = 0, i\omega = 0)$, which can be calculated with Eqs. (A8)–(A16), we can check the validity of the approximation for the irreducible vertices.

Another method is to check the f-sum rule. The present theory, SCSOPT, is a conserving approximation and the calculated response functions must satisfy the f-sum rule. The f-sum rule reads

$$\langle\langle \omega \rangle\rangle_{\rm C} = \langle\langle \omega \rangle\rangle_{\rm S} = F(\boldsymbol{q}), \tag{37}$$

where

$$\langle\langle \omega \rangle\rangle_\mu = \int_{-\infty}^{\infty} d\omega \omega M(\boldsymbol{q},\omega) \quad (M,\mu = C,S) \tag{38}$$

and

$$F(\boldsymbol{q}) = \frac{1}{2N} \sum_{\mathbf{k}} [\epsilon_{\boldsymbol{k}+\boldsymbol{q}} + \epsilon_{\boldsymbol{k}-\boldsymbol{q}} - 2\epsilon_{\boldsymbol{k}}] \sum_\sigma G_\sigma(\boldsymbol{k}, 0-). \tag{39}$$

In particular, for $\epsilon_{\boldsymbol{k}} = k^2/(2m)$, $F(q) = q^2/(2m)$. Note that we have defined susceptibilities (and structure factors) as those per particle (not per lattice point). Therefore, the f-sum rule can be rewritten as

$$-\frac{\partial}{\partial\tau} \chi_{\rm c}(\boldsymbol{q},\tau)\Big|_{\tau=0} = -\frac{\partial}{\partial\tau} \chi_{\rm s}(\boldsymbol{q},\tau)\Big|_{\tau=0} = F(\boldsymbol{q}). \tag{40}$$

Note that

$$\begin{aligned}\frac{\partial^n}{\partial\tau^n} \chi_\mu(\boldsymbol{q},\tau)\Big|_{\tau=0} &= (-1)^n \int_{-\infty}^{\infty} d\omega\, \omega^n M(\boldsymbol{q},\omega) \\ &= (-1)^n \langle\langle \omega^n \rangle\rangle_\mu.\end{aligned} \tag{41}$$

[See Eq. (35).] A merit of this form of the f-sum rule, Eq. (40), is that we can calculate it without analytic continuation from the imaginary axis to the real axis.

We have found that the compressibility sum rule is satisfied very accurately and the effect of the vertex corrections is not very significant. However, for the counterpart for the spin density, the equality is well satisfied only with the vertex corrections. We have also found that the vertex corrections make the f-sum rule be satisfied satisfactorily. Thus, we have confirmed that the present approximation for the vertex corrections works well. More details are given in the Appendix.

Finally, we note that the structure factors $C(\boldsymbol{q})$ and $S(\boldsymbol{q})$ are equal to the response functions at $\tau = 0$,

$$M(\boldsymbol{q}) = \int_{-\infty}^{\infty} d\omega M(\boldsymbol{q},\omega) = \chi_{\mu}(\boldsymbol{q},\tau = 0). \tag{42}$$

We mainly use a lattice whose size is $N_{\rm L} = 128 \times 128$ and $M = 1024$ Matsubara frequencies. We have also carried out a few calculations using a larger lattice ($N_{\rm L} = 256 \times 256$) and found that results are unaffected by the finite-size effect. Results obtained on the imaginary axis are analytically continued to the real axis with the Padé approximation.

III. RESULTS

We mainly show results obtained $v_1 = V_1/(4\pi t) = 0.5u$ and $v_2 = V_2/(4\pi t) = 0.2u$, where $u = U/(4\pi t)$. Here, $1/(4\pi t)$ is the density of states per lattice point and spin in the dilute limit. We also use other parameters having different ratio, for example, with negative v_2, but qualitative feature remains intact as long as v_1, $|v_2|$ is much smaller than u. The wave vector dependence of $U + V(q)$ is shown in the inset of Fig. 3.

Figure 3 shows the quasiparticle dispersion $E(k)$ determined by solving the equation

$$E(\boldsymbol{k}) = \epsilon_{\boldsymbol{k}} - \mu + \Sigma(\boldsymbol{k}, E(\boldsymbol{k})) \tag{43}$$

and the damping rate $\gamma(\boldsymbol{k})$,

$$\gamma(\boldsymbol{k}) = -2{\rm Im}\Sigma(\boldsymbol{k}, E(\boldsymbol{k})). \tag{44}$$

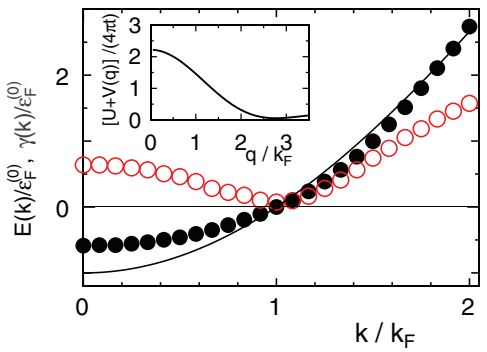

FIG. 3. (Color online) Quasiparticle dispersion $E(\boldsymbol{k})$ (solid dots) and the damping rate $\gamma(\boldsymbol{k})$ (open dots) for $u = 0.30$. Solid line stands for the free dispersion $\xi_{\boldsymbol{k}} = \epsilon_{\boldsymbol{k}} - \mu$. The inset shows the wave-vector dependence of the interaction $U + V(\boldsymbol{q})$ with $u = 0.30, v_1 = 0.15$, and $v_2 = 0.06$.

The dispersion is narrowed by the interaction. The effective mass m^* can be calculated by

$$\frac{m^*}{m} = \frac{1 - \frac{\partial\Sigma}{\partial\omega}\big|_{k=k_{\rm F},\omega=0}}{1 + \frac{m}{\hbar^2 k_{\rm F}}\frac{\partial\Sigma}{\partial k}\big|_{k=k_{\rm F},\omega=0}}. \tag{45}$$

For $u = 0.30$, $m^*/m \simeq 1.4$, and for $u = 0.50$, $m^*/m \simeq 2.5$. The effective mass is enhanced by the correlation, but is not so much enhanced as in 2D ^{3}He at $\rho = 4.9\ {\rm nm}^{-2}$ ($m^*/m \simeq 4$),[18] where the neutron experiment was performed. It should also be noted that the damping becomes large as the wave vector deviates from the Fermi wave vector and is comparable to the (bare) Fermi energy at $|k - k_{\rm F}| \simeq k_{\rm F}$. This large damping was also found in previous studies.[11,12] Although the dispersion at large wave vectors is little affected by the interaction, quasiparticles are far from free particles. They suffer from strong damping. In addition to the mass enhancement, this damping also significantly affects the dynamical structure factors at large wave vectors as we shall see.

A. Dynamical structure factors $C(\boldsymbol{q},\omega)$ and $S(\boldsymbol{q},\omega)$

Figure 4 shows the dynamical structure factors $C(\boldsymbol{q},\omega)$, Eq. (32), and $S(\boldsymbol{q},\omega)$, Eq. (33), at $q = 0.5k_{\rm F}$. We also show the dynamical structure factor in the noninteracting case. We can see that a peak develops in $C(\boldsymbol{q},\omega)$ above the p-h continuum in the noninteracting case. This peak corresponds to the zero sound mode. In Fig. 5(a), $C(\boldsymbol{q},\omega)$ for different values of u is shown. As u increases, the peak position shifts to a higher energy, its intensity decreases, and the width increases. It can also be seen that the effect of vertex correction is essential to obtain the zero sound peak [Fig. 5(a)]. In the limit of $q \to 0$, the width of the zero sound mode should vanish, but it can be finite at a small but finite wave vector. We should note that the height and width of the peak can be quantitatively affected by the partial neglect of vertex corrections. As is shown in the Appendix, the effect of the partial neglect is most serious in the long-wavelength limit.

A peak, the paramagnon peak, also develops in the spin fluctuation spectrum $S(\boldsymbol{q},\omega)$ [Fig. 5(b)]. The peak appears in the continuum and has finite width. In inelastic neutron scattering, one can observe a spectrum of a two-peak structure

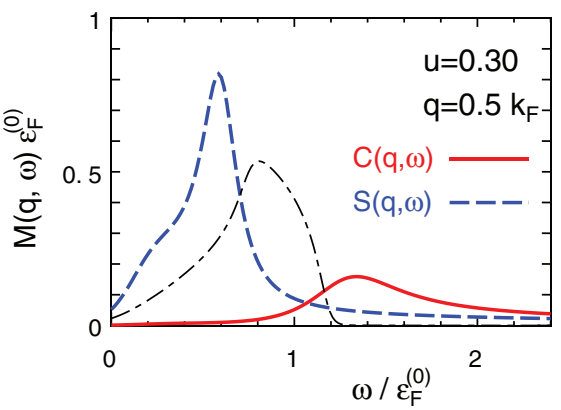

FIG. 4. (Color online) Dynamical structure factors $C(\boldsymbol{q},\omega)$ (solid line) and $S(\boldsymbol{q},\omega)$ (dashed line) at $u = 0.30$ and $q = 0.5k_{\rm F}$. For comparison, the result at $u = 0$ is also shown (dash-dotted line).

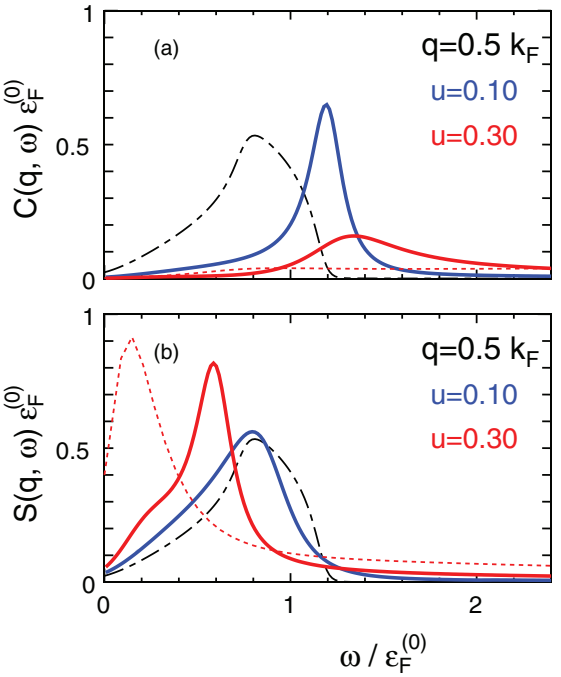

FIG. 5. (Color online) (a) Dynamical structure factor $C(\boldsymbol{q},\omega)$ at $q = 0.5k_{\mathrm{F}}$ for different values of u: $u = 0.0$ (dash-dotted line), 0.10 (blue line), and 0.30 (red line). Dotted line shows the result at $u = 0.30$ without vertex corrections. (b) Dynamical structure factor $S(\boldsymbol{q},\omega)$ at $q = 0.5k_{\mathrm{F}}$ for different values of u: $u = 0.0$ (dash-dotted line), 0.10 (blue line), and 0.30 (red line). Dotted line shows the result at $u = 0.30$ without vertex corrections.

in the long-wavelength region. The relative strength of the peaks depends on the ratio of intensities of coherent and incoherent scatterings.

We note that the p-h threshold (in the noninteracting case) has little relevance once the interaction sets in. There is no marked structure at the threshold. This is because of the multiple scattering. Mathematically, the effect appears through (the imaginary part of) the self-energy and the vertex corrections. Crudely speaking, the imaginary part of the self-energy (damping) simply smears the spectrum. The vertex corrections can partly cancel out the effect damping and lead to the correct spectrum. This is clearly seen in Fig. 5(a), for example. To obtain the correct spectrum, both effects have to be properly considered.

Figure 6 shows the dynamical structure factors at $q = 2.0k_{\mathrm{F}}$. At this wave vector, the p-h continuum extends to $\omega = 0$. $C(\boldsymbol{q},\omega)$ and $S(\boldsymbol{q},\omega)$ are similar in shape, and the intensity shifts to low energies. The effect of vertex corrections is found to be still significant as can be seen in Figs. 7(a) and 7(b).

Finally, we show $C(\boldsymbol{q},\omega)$ and $S(\boldsymbol{q},\omega)$ at a short wavelength, $q = 3.0k_{\mathrm{F}}$, in Fig. 8. For comparison, the spectrum in the noninteracting case is also shown. The spectrum at $u = 0.0$ has lower and upper thresholds and is asymmetric. This asymmetry is caused by the lattice effect. Although we consider the dilute limit, the lattice effect is inevitable in the large-wave-vector and high-energy region. In the continuum model, the spectrum in the noninteracting case is more symmetric at $q = 3k_{\mathrm{F}}$.

As the interaction increases, we find that the peak in $C(\boldsymbol{q},\omega)$ shifts to low energy (see also Fig. 9), and the spectrum becomes

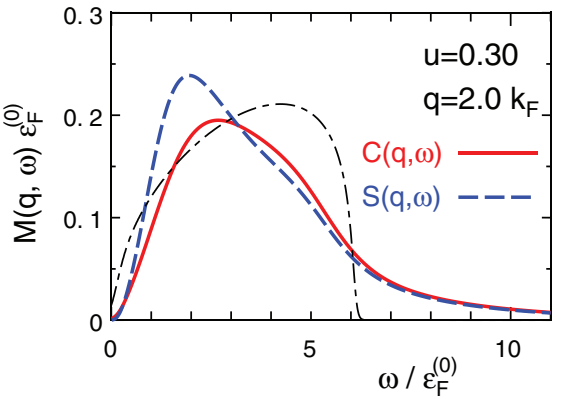

FIG. 6. (Color online) Dynamical structure factors $C(\boldsymbol{q},\omega)$ (solid line) and $S(\boldsymbol{q},\omega)$ (dashed line) at $u = 0.30$ and $q = 2.0k_{\mathrm{F}}$. For comparison, the result at $u = 0$ is also shown (dash-dotted line).

finite even below the lower threshold of the p-h continuum because of the multiple scattering. Note that at $q = 3k_{\mathrm{F}}$, quasiparticles far away from the Fermi surface, $k - k_{\mathrm{F}} \simeq k_{\mathrm{F}}$, which suffer from large damping, contribute to the spectrum. In the parameter region we studied, we cannot find a peak developing below the lower threshold, but the intensity is clearly accumulating at lower energies. The present peak reflects development of short-range density correlation, but its width is so large that it does not correspond to a well-defined mode such as the roton mode in superfluid ^{4}He. See also the next subsections.

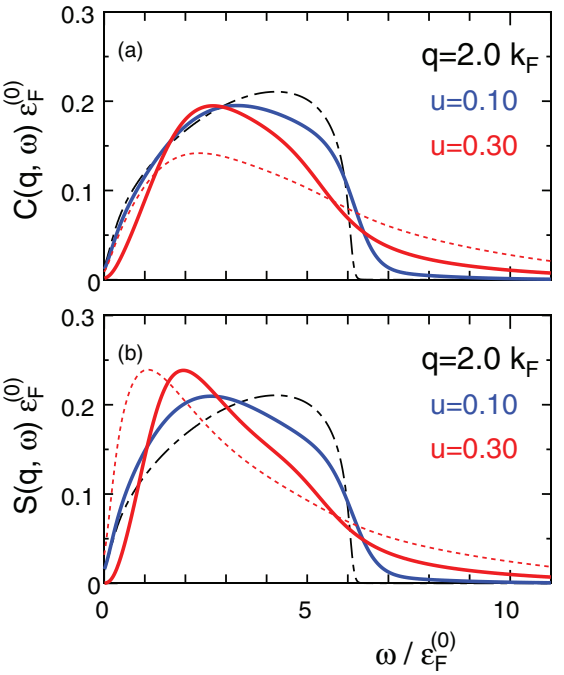

FIG. 7. (Color online) (a) Dynamical structure factor $C(\boldsymbol{q},\omega)$ at $q = 2.0k_{\mathrm{F}}$ for different values of u: $u = 0.0$ (dash-dotted line), 0.10 (blue line), and 0.30 (red line). Dotted line shows $C(\boldsymbol{q},\omega)$ at $u = 0.30$ without vertex corrections. (b) Dynamical structure factor $S(\boldsymbol{q},\omega)$ at $q = 2.0k_{\mathrm{F}}$ for different values of u: $u = 0.0$ (dash-dotted line), 0.10 (blue line), and 0.30 (red line). Dotted line shows $S(\boldsymbol{q},\omega)$ at $u = 0.30$ without vertex corrections.

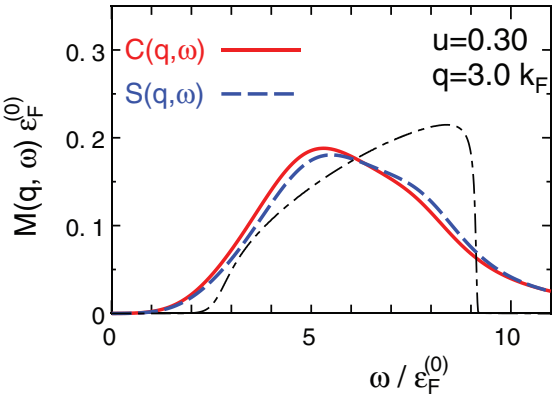

FIG. 8. (Color online) Dynamical structure factors $C(\boldsymbol{q},\omega)$ (solid line) and $S(\boldsymbol{q},\omega)$ (dashed line) at $u = 0.30$ and $q = 3.0k_{\mathrm{F}}$. For comparison, the result at $u = 0$ is also shown (dash-dotted line).

The peak position in $S(\boldsymbol{q},\omega)$ is similar to that in $C(\boldsymbol{q},\omega)$. Therefore, only a single peak will be observed in neutron scattering at this wave vector. In other words, not only density fluctuations but also spin fluctuations can contribute to a single peak at low frequencies.

The effect of vertex corrections is also evident at $q = 3.0k_{\mathrm{F}}$ (Fig. 9), but is modest compared with long-wavelength regions. For example, only the peak height is found to be modestly changed by the vertex corrections.[19]

B. Collective mode dispersion

We plot the peak frequency of $C(\boldsymbol{q},\omega)$ [$S(\boldsymbol{q},\omega)$] and its FWHM (full width at half maximum) $\Gamma(\boldsymbol{q})$ in Fig. 10(a) [Fig. 10(b)]. It can be seen that the zero sound mode appears just above the p-h threshold in the long-wave regime and it enters the continuum at $q \simeq k_{\mathrm{F}}$. Then, the peak broadens significantly [$E_{\mathrm{peak}}(q) \lesssim \Gamma(q)$] and cannot be regarded as a well-defined mode any more. It is remarkable that $E_{\mathrm{peak}}(q)$ exhibits a downturn and has a minimum at $q \simeq 2k_{\mathrm{F}}$. As u increases, the minimum shifts to a larger q, but it is still in the continuum at $u = 0.50$. Thus, we find no well-defined density collective mode in the short-wavelength regime, but

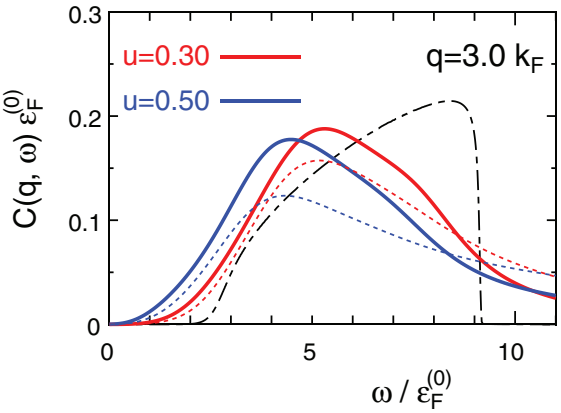

FIG. 9. (Color online) Dynamical structure factor $C(\boldsymbol{q},\omega)$ at $q = 3.0k_{\mathrm{F}}$ for different values of u: $u = 0.0$ (dash-dotted line), 0.30 (red lines), and 0.50 (blue lines). Dotted lines show results without vertex corrections.

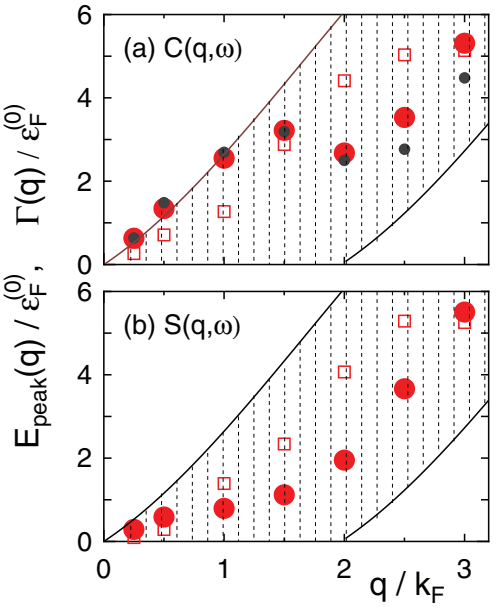

FIG. 10. (Color online) (a) The peak frequency $E_{\mathrm{peak}}(\boldsymbol{q})$ (closed dots) of $C(\boldsymbol{q},\omega)$ as a function of q at $u = 0.30$. Small dots represent the results at $u = 0.50$. Open squares stand for the FWHM $\Gamma(\boldsymbol{q})$ at $u = 0.30$. Dotted region is the p-h continuum in the noninteracting case. (b) The peak frequency $E_{\mathrm{peak}}(\boldsymbol{q})$ (closed dots) of $S(\boldsymbol{q},\omega)$ as a function of q at $u = 0.30$. Open squares stand for the FWHM $\Gamma(\boldsymbol{q})$. Dotted region is the p-h continuum in the noninteracting case.

the dispersion of the obtained peak frequency is in qualitative agreement with the experimental finding.

In contrast to the case with $C(\boldsymbol{q},\omega)$, the peak in $S(\boldsymbol{q},\omega)$ is in the continuum for any q. However, in the long-wavelength regime, $\Gamma(q) < E_{\mathrm{peak}}(q)$, and the mode is well defined (the paramagnon mode). As q increases, $\Gamma(q)$ significantly increases and the mode is no longer well defined. In contrast to the case with $C(\boldsymbol{q},\omega)$, $E_{\mathrm{peak}}(q)$ has no clear downturn although it has an inflection point.

C. Structure factors $C(\boldsymbol{q})$ and $S(\boldsymbol{q})$

Finally, we discuss the structure factors $C(\boldsymbol{q})$ and $S(\boldsymbol{q})$. Figure 11 shows the change in the structure factors caused by the interaction, $\Delta M(\boldsymbol{q}) = M(\boldsymbol{q})_{u>0} - M(\boldsymbol{q})_{u=0}$ ($M = C,S$). It can be seen that the density fluctuations are suppressed in the long-wavelength region, but are enhanced at $q > 2.0k_{\mathrm{F}}$. Without interaction, the structure factor $M(\boldsymbol{q})$ is given by[23]

$$M(\boldsymbol{q}) = \begin{cases} \frac{2}{\pi}\left[\frac{q}{2k_{\mathrm{F}}}\sqrt{1-\left(\frac{q}{2k_{\mathrm{F}}}\right)^2} + \arcsin\frac{q}{2k_{\mathrm{F}}}\right], & 0 \leqslant q < 2k_{\mathrm{F}}, \\ 1, & q \geqslant 2k_{\mathrm{F}}. \end{cases} \tag{46}$$

At $0 \leqslant q \leqslant 2k_{\mathrm{F}}$, $M(q)$ is convex upward. Therefore, the minimum in $\Delta C(\boldsymbol{q})$ at $q \simeq 1.2k_{\mathrm{F}}$ causes a weak shoulder structure in $C(\boldsymbol{q})$ at a small wave vector. A peak in $C(\boldsymbol{q})$ at a large wave vector implies that the interaction tends to enhance crystalline ordering whose characteristic wave vector is larger than $2k_{\mathrm{F}}$. For the interaction strength studied here, the enhancement is weak, but if this short-range order develops further, the enhancement of $C(\boldsymbol{q})$ at large wave vectors will become significant. Correspondingly, $\Gamma(q)$ at $q > 2k_{\mathrm{F}}$ will

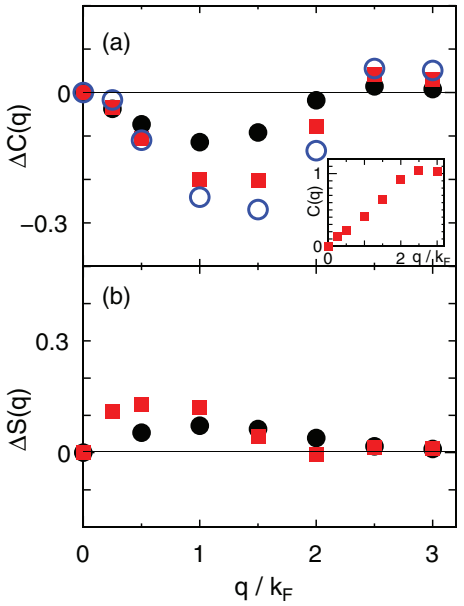

FIG. 11. (Color online) Difference $\Delta M(\boldsymbol{q})$ between structure factor $M(\boldsymbol{q})$ at finite u and at $u = 0$, $\Delta M(\boldsymbol{q}) = M(\boldsymbol{q})|_{u>0} - M(\boldsymbol{q})|_{u=0}$. (a) $M = C$ and (b) $M = S$. Closed dots represent results at $u = 0.10$, squares at $u = 0.30$, and open dots at $u = 0.50$. The inset shows $C(\boldsymbol{q})$ at $u = 0.30$.

decrease and the peak $C(\boldsymbol{q},\omega)$ at $q > 2k_F$ will also become prominent. Indeed, in the previous theoretical studies using realistic interaction potential,[22,24] a more prominent peak in $C(\boldsymbol{q})$ is observed at $q \simeq 3k_F$, in fair agreement with experiment.[24]

On the other hand, the spin structure factor $S(\boldsymbol{q})$ is enhanced, in particular, in the long-wavelength region by the interaction. At $q \gtrsim 2k_F$, the enhancement is insignificant, and $S(\boldsymbol{q})$ and $C(\boldsymbol{q})$ are similar in magnitude in this region, in agreement with the results in the previous sections. This behavior of $S(\boldsymbol{q})$ is qualitatively consistent with the results obtained with the diffusion Monte Carlo method.[22]

IV. SUMMARY AND DISCUSSION

We have calculated the dynamical responses of an interacting 2D fermion system treating the short-ranged interaction with the self-consistent second-order perturbation theory (SCSOPT). At a small wave vector, we have found a peak in the dynamical density structure factor $C(\boldsymbol{q},\omega)$ corresponding to the zero sound, and also a peak in the dynamical spin structure factor $S(\boldsymbol{q},\omega)$ corresponding to the paramagnon mode. On the other hand, at a large wave vector, $q = 3.0k_F$, we have found that the spectrum extends beyond the p-h threshold in the noninteracting case. A peak in $C(\boldsymbol{q},\omega)$ shifts to a lower frequency as interaction strength increases. However, the peak is not so sharp, and it does not correspond to a well-defined propagating mode.

Now, we discuss the relevance of the present results to the experimental finding by Godfrin *et al.* and its theoretical interpretation.[1,2] They found a clear peak in the neutron spectrum at $\omega \simeq 2.5\epsilon_F^{(0)}$, which is below the p-h threshold, at $q \simeq 3k_F$. The width of the peak was found to be smaller than or equal to the experimental energy resolution, $\Delta E = 0.1\,\mathrm{meV} \simeq 0.5\epsilon_F^{(0)}$. A peak found at $q = 3k_F$ in $C(\boldsymbol{q},\omega)$ in this study is located at $\omega \simeq 5\epsilon_F^{(0)}$, at an energy much larger than that found in the experiment. Although we found a downturn of the peak frequency as a function of wave vector, the width of the peak is so large that it cannot be considered a well-defined mode. This discrepancy must mainly stem from the use of a model Hamiltonian. For example, at a large wave vector, the lattice effect is inevitable. Moreover, our model interaction potential may not be a good approximation to a realistic effective potential. If the low-energy mode found by Godfrin *et al.* is similar in nature to the roton mode in superfluid ^{4}He, as is suggested by the authors, it is likely that it represents the tendency of the system towards crystallization.[21] It is clear that as we have not taken account of the hard-core effect, we underestimate the tendency of the system towards crystallization, that is, the structure factors $C(\boldsymbol{q},\omega)$ and $C(\boldsymbol{q})$ at large wave vectors. The experimental finding implies that 2D ^{3}He has stronger short-ranged crystalline ordering than the present effective Hamiltonian describes.

On the other hand, we can make a few points from the present study. One is that, as the quasiparticles far away from the Fermi surface suffer from strong damping, the p-h threshold in the noninteracting case has little relevance (except in the long-wavelength limit), and the spectrum extends outside the threshold without any significant structures at the threshold. This is in contrast to the result of the dynamical many-body theory used in Refs. 1 and 2. In the dynamical many-body theory, an energy-dependent effective interaction is introduced, and the RPA expression of $C(\boldsymbol{q},\omega)$ is generalized with energy-dependent effective interaction. However, the damping effect on the quasiparticle dispersion is not considered (at least explicitly), and the p-h threshold remains intact even in the presence of the interaction. The intensity then accumulates just above the lower p-h threshold at $q \simeq 3k_F$. Introduction of the damping necessarily makes the spectrum extend beyond the p-h thresholds and also make the spectrum broad. Indeed, in Ref. 10, the effect of the damping is partially considered and the broadening of the peak is observed. In the present study, we find that the damping rate $\gamma(k) \simeq \epsilon_F^{(0)}$ at $|k - k_F| \simeq k_F$. This large damping was also obtained in the previous theoretical studies of bulk ^{3}He,[11–13] and it resulted in the smooth dynamical structure factor without marked structures at the threshold.[12,13] With this large damping, it might be difficult for a well-defined mode to evolve at a large wave vector. Actually, in those studies,[11–13] the self-consistency of the Green's function (or the single-particle energy) and the self-energy was only partially achieved. It is possible that the full self-consistent T-matrix calculation will result in smaller damping of quasiparticles and a sharp peak in $C(\boldsymbol{q},\omega)$ at large wave vectors. At any rate, it must be necessary to consider both the self-energy effect and the vertex corrections self-consistently.

Another point implied by the present study is the importance of the spin fluctuations. Indeed, the spin susceptibility is significantly enhanced in 2D,[18] and the effect of spin fluctuations was found to be important in enhancing the effective mass in the quantum Monte Carlo simulation.[22] It is then natural that the spin fluctuations also contribute

significantly to the dynamical structure factor. The dynamical spin structure factor $S(\boldsymbol{q},\omega)$ is indeed found to be dominant over $C(\boldsymbol{q},\omega)$ at a small wave vector. $S(\boldsymbol{q},\omega)$ contributes to the neutron scattering cross section as an incoherent part. The ratio of the incoherent part to the coherent part $C(\boldsymbol{q},\omega)$ is estimated to be approximately 0.25 in bulk ^{3}He.[25] If it is similar in magnitude in 2D, then we can observe two peaks in the neutron cross scattering cross section at small wave vectors, as was indeed observed in 3D,[5] if the background subtraction can be precisely performed. On the other hand, at large wave vectors, $S(\boldsymbol{q},\omega)$ is found to be similar in magnitude to $C(\boldsymbol{q},\omega)$ in the present study. Although it is possible that the $C(\boldsymbol{q},\omega)$ is dominant over $S(\boldsymbol{q},\omega)$ with more realistic potential, quantitative agreement will be obtained only after taking account of the spin fluctuations. It should be noted that the exchange processes must be considered in calculating $S(\boldsymbol{q},\omega)$ reliably as was mentioned in the Introduction.

To summarize, it is still a challenging problem to explain the surprising finding of Godfrin *et al.*[1,2] The existence of a sharp mode at a large wave vector implies the development of short-range crystalline order. We believe that much more effort will be necessary to explain it microscopically.

ACKNOWLEDGMENT

D.S.H. is supported by JSPS KAKENHI Grant No. 24540343.

APPENDIX: SELF-ENERGY AND VERTEX CORRECTIONS

The Hartree term is expressed as

$$\Sigma_\sigma^{(H)} = Un_{-\sigma} + V(0)n. \tag{A1}$$

The Fock term is expressed as

$$\Sigma_\sigma^{(F)}(\boldsymbol{k}) = \sum_{k'} V(\boldsymbol{k}-\boldsymbol{k}')G_\sigma(k'). \tag{A2}$$

Using the Fourier transformation, we find

$$\begin{aligned}\Sigma_\sigma^{(F)}(\boldsymbol{k}) = {} & 2V^{(1)}G_\sigma(\boldsymbol{\delta}^{(1)},0-)(\cos k_x + \cos k_y) \\ & + 2V^{(2)}G_\sigma(\boldsymbol{\delta}^{(2)},0-)[\cos(k_x+k_y)+\cos(k_x-k_y)] \\ & + 2V^{(3)}G_\sigma(\boldsymbol{\delta}^{(3)},0-)(\cos 2k_x + \cos 2k_y) \\ & + 2V^{(4)}G_\sigma(\boldsymbol{\delta}^{(4)},0-)[\cos(2k_x+k_y) \\ & + \cos(2k_x-k_y)+\cos(k_x+2k_y) \\ & + \cos(k_x-2k_y)],\end{aligned} \tag{A3}$$

where $\boldsymbol{\delta}^{(n)}$ is the position of one of the nth neighbors.

In the coordinate space, the second-order self-energy $\Sigma_\sigma^{(2)}$ is expressed as

$$\begin{aligned}\Sigma_\sigma^{(2)}(r) = {} & -U^2 G_\sigma(r)G_{-\sigma}(r)G_{-\sigma}(-r) \\ & - \sum_J UV^{(n)}G_\sigma(r)G_{-\sigma}(\boldsymbol{r}_{J+},\tau)G_{-\sigma}(-\boldsymbol{r}_{J+},-\tau) \\ & - \sum_J V^{(n)}UG_\sigma(r)G_{-\sigma}(\boldsymbol{r}_{J-},\tau)G_{-\sigma}(-\boldsymbol{r}_{J-},-\tau) \\ & - \sum_{J,J',\sigma'} V^{(n)}V^{(n')}G_\sigma(r)G_{\sigma'}(\boldsymbol{r}_{J+J'-},\tau) \\ & \times G_{\sigma'}(-\boldsymbol{r}_{J+J'-},-\tau)\end{aligned}$$

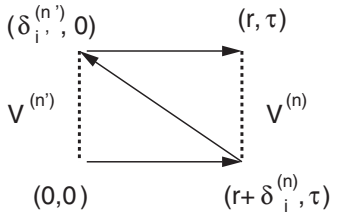

FIG. 12. Diagram for a second-order self-energy term in the coordinate representation. Solid lines represent the single-particle Green's function $G(k)$ and dotted lines the interaction.

$$+ \sum_{J,J'} V^{(n)}V^{(n')}G_\sigma(\boldsymbol{r}_{J+},\tau)G_\sigma(\boldsymbol{r}_{J'-},\tau) \times G_\sigma(-\boldsymbol{r}_{J+J'-},-\tau), \tag{A4}$$

where $r = (\boldsymbol{r},\tau)$, $J = (n,j)$, $J' = (n',j')$,

$$\boldsymbol{r}_{J\pm} = \boldsymbol{r} \pm \boldsymbol{\delta}_J = \boldsymbol{r} \pm \boldsymbol{\delta}_j^{(n)}, \tag{A5}$$

and

$$\boldsymbol{r}_{JsJ's'} = \boldsymbol{r} + s\boldsymbol{\delta}_J + s'\boldsymbol{\delta}_{J'}, \quad s,s' = \pm, \tag{A6}$$

with $\boldsymbol{\delta}_J = \boldsymbol{\delta}_j^{(n)}$ being vectors connecting the nth neighbor pairs; $j = 1 \sim 4$ for $n = 1,2,3$ and $j = 1 \sim 8$ for $n = 4$. Correspondingly, J runs from 1 to 20. The diagram corresponding to the last term is shown in Fig. 12. $\Sigma_\sigma(k)$ is readily obtained from $\Sigma_\sigma(r)$ with the Fourier transformation.

The full polarization function $P_\mu(q)$ $[=\chi_\mu(q)/2]$ is expressed in terms of irreducible polarization function $\overline{P}_\mu(q)$ as

$$\begin{aligned}P_{\rm c}(q) = {} & \overline{P}_{\rm c}(q) - \overline{P}_{\rm c}(q)[U+2V(\boldsymbol{q})]P_{\rm c}(q) \\ & + \frac{1}{N}\sum_{\boldsymbol{k}}\frac{1}{N}\sum_{\boldsymbol{k}'}\overline{P}_{\rm c}(q;\boldsymbol{k})V(\boldsymbol{k}-\boldsymbol{k}')P_{\rm c}(q;\boldsymbol{k}')\end{aligned} \tag{A7}$$

[Fig. 2(a)]. The third term on the right-hand side represents the exchange processes. The spin polarization function $P_{\rm s}(q)$ satisfies a similar equation except for the replacement of $-[U+2V(\boldsymbol{q})]$ by $+U$. Equation (A7) can be rewritten as

$$\begin{aligned}P_{\rm c}(q) = {} & \overline{P}_{\rm c}(q) - \overline{P}_{\rm c}(q)[U+2V(\boldsymbol{q})]P_{\rm c}(q) \\ & + \sum_J \overline{P}_{{\rm c};J}(q)V^{(n)}P_{{\rm c};J}(q),\end{aligned} \tag{A8}$$

where

$$P_{{\rm c};J}(q) = \frac{1}{N}\sum_{\boldsymbol{k}} e^{i\boldsymbol{k}\cdot\boldsymbol{\delta}_J}P_{\rm c}(q,\boldsymbol{k}). \tag{A9}$$

Here, we abbreviate (n,j) by J and $\boldsymbol{\delta}_J = \boldsymbol{\delta}_j^{(n)}$. The equation for $P_{{\rm c};J}(q)$ is similarly obtained,

$$\begin{aligned}P_{{\rm c};J}(q) = {} & \overline{P}_{{\rm c};J}(q) - \overline{P}_{{\rm c};J}(q)[U+2V(\boldsymbol{q})]P_{\rm c}(q) \\ & + \sum_{J,J'}\overline{P}_{{\rm c};J,J'}(q)V^{(n')}P_{{\rm c};J'}(q),\end{aligned} \tag{A10}$$

where

$$\overline{P}_{\mu;J,J'}(q) = \frac{1}{N}\sum_{\boldsymbol{k}} e^{-i\boldsymbol{k}\cdot(\boldsymbol{\delta}_J-\boldsymbol{\delta}_{J'})}\overline{P}_\mu(q;\boldsymbol{k}), \tag{A11}$$

$J=(n,j)$, and $J'=(n',j')$. Equations (A8) and (A10) are equations in an $N_{nn}\times N_{nn}$ matrix form; in the present case, $N_{nn}=21$.

Irreducible polarization functions $\overline{P}_\mu(q)$ and $\overline{P}_{\mu;J}(q)$ are expressed in terms of three-point vertex functions $\Lambda_\mu(k,q)$ and $\Lambda_{\mu;J}(k;q)$ as

$$\overline{P}_\mu(q)=-\sum_k G_\sigma(k+q)G_\sigma(k)\Lambda_\mu(k;q), \quad \text{(A12)}$$

$$\overline{P}_{\mu;J}(q)=-\sum_k G_\sigma(k+q)G_\sigma(k)\Lambda_{\mu;J}(k;q), \quad \text{(A13)}$$

and

$$\overline{P}_{\mu;J,J'}(q)=-\sum_k e^{i\boldsymbol{k}\cdot\boldsymbol{\delta}_J}G_\sigma(k+q)G_\sigma(k)\Lambda_{\mu;J'}(k;q). \quad \text{(A14)}$$

Three-point vertex functions satisfy the following integral equations [Fig. 2(b)],

$$\Lambda_\mu(k;q)=1+\sum_{k'}\gamma_\mu(k,k';q)G(k'+q)G(k')\Lambda_\mu(k';q) \quad \text{(A15)}$$

and

$$\Lambda_{\mu;J'}(k;q)=e^{-i\boldsymbol{k}\cdot\boldsymbol{\delta}_{J'}}+\sum_{k'}\gamma_\mu(k,k';q)\times G(k'+q)G(k')\Lambda_{\mu;J'}(k';q). \quad \text{(A16)}$$

Once p-h irreducible vertices $\gamma_\mu(k,k';q)$ are obtained, we can calculate three-point vertex functions Λ by solving Eqs. (A15) and (A16). We then find irreducible polarization functions $\overline{P}_\mu$ using Eqs. (A12)–(A14). Finally, we obtain $P_\mu(q)$ by solving the matrix equation, Eqs. (A8) and (A10). Now that irreducible vertices are given in Fig. 2, we can in principle calculate $P_\mu(q)$. However, there is still a technical difficulty, and we resort to a further approximation.

We can efficiently solve integral equations that are of a convolution form, $F(k)=\sum_{k'}K(k\pm k')H(k')F(k')$, using the fast Fourier transformation (FFT). Unfortunately, the integral equations for Λ's does not necessarily take a convolution form. In general, $\gamma(k,k';q)$ is not a function of $k\pm k'$. This stems from terms involving $V(\boldsymbol{q})$. With only U, the integral equation for $\Lambda_\mu(k;q)$ is a convolution form and can be easily solved. Thus, we make further approximations for $\gamma(k,k';q)$. As the problem is concerned only with wave vectors, we suppress frequencies (or imaginary times) in the argument of γ. First, we take Fourier transformation of $\gamma_\mu(\boldsymbol{k},\boldsymbol{k}';\boldsymbol{q})$ (see Fig. 13),

$$\gamma_\mu(\boldsymbol{R},\boldsymbol{R}';\boldsymbol{r})=\frac{1}{N_{\rm L}^3}\sum_{\boldsymbol{k},\boldsymbol{k}',\boldsymbol{q}}e^{i(\boldsymbol{k}\cdot\boldsymbol{R}-\boldsymbol{k}'\cdot\boldsymbol{R}'+\boldsymbol{q}\cdot\boldsymbol{r})}\gamma(\boldsymbol{k},\boldsymbol{k}';\boldsymbol{q}). \quad \text{(A17)}$$

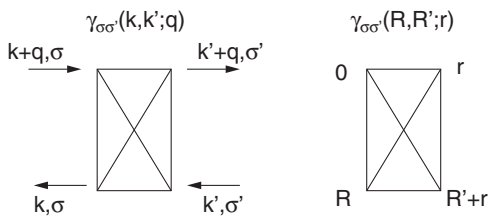

FIG. 13. p-h irreducible vertex function $\gamma(k,k';q)$ and its Fourier transform $\gamma(R,R';r)$.

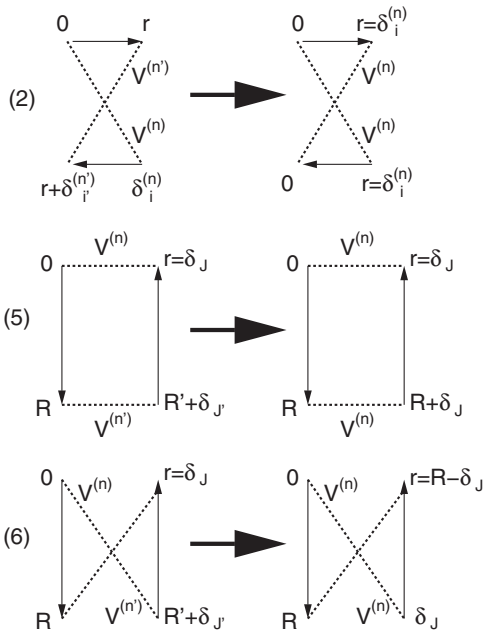

FIG. 14. Approximations for p-h irreducible vertices $\gamma^{(i)}_{\sigma\sigma'}(\boldsymbol{R},\boldsymbol{R}';\boldsymbol{r})$ ($i=2,5$, and 6).

We can easily show that, if $\boldsymbol{r}$ and $\boldsymbol{R}$ (or $\boldsymbol{R}'$) are independent of each other and if $\gamma_\mu(\boldsymbol{R},\boldsymbol{R}';\boldsymbol{q})=0$ for $\boldsymbol{R}\pm\boldsymbol{R}'\neq 0$, then $\gamma_\mu(\boldsymbol{k},\boldsymbol{k}';\boldsymbol{q})=\gamma_\mu(\boldsymbol{k}\pm\boldsymbol{k}';\boldsymbol{q})$. We can readily see that $\gamma^{(1)}_{\sigma\sigma}(\boldsymbol{R},\boldsymbol{R}';\boldsymbol{r})=\gamma^{(1)}_{\sigma\sigma}(\boldsymbol{R},\boldsymbol{R};\boldsymbol{0})\delta_{\boldsymbol{R},\boldsymbol{R}'}\delta_{\boldsymbol{r},\boldsymbol{0}}$; that is, it automatically satisfied the condition $\boldsymbol{R}=\boldsymbol{R}'$. We need no approximation for this term,

$$\gamma^{(1)}_{\sigma\sigma'}(k,k;q)=\delta_{\sigma\sigma'}\gamma^{(1)}(k-k')=\delta_{\sigma\sigma'}[U+V(\boldsymbol{k}-\boldsymbol{k}')]^2P_0(k-k'). \quad \text{(A18)}$$

$\gamma^{(2)}_{\sigma\sigma}$ involves only $V(\boldsymbol{q})$. In coordinate space, it is expressed as in Fig. 14. We see that $\boldsymbol{R}=\boldsymbol{r}+\boldsymbol{\delta}_{J'}$ and $\boldsymbol{R}'=\boldsymbol{\delta}_J-\boldsymbol{r}$; that is, $\boldsymbol{r}$ and $\boldsymbol{R}$ are not independent of each other. In this case, $\gamma^{(2)}_{\sigma\sigma}$ cannot be a function of $\boldsymbol{k}\pm\boldsymbol{k}'$ even if we restrict to the case $\boldsymbol{R}=\pm\boldsymbol{R}'$. We then apply a local approximation to $\gamma^{(2)}$, that is, $n=n'$ and $\boldsymbol{\delta}_J=-\boldsymbol{\delta}_{J'}=\boldsymbol{r}$. Then $\gamma^{(2)}_{\sigma\sigma}(\boldsymbol{k},\boldsymbol{k}';\boldsymbol{q})$ becomes independent of $\boldsymbol{k}$ and $\boldsymbol{k}'$,

$$\gamma^{(2)}_{\sigma\sigma'}(k,k';q)\simeq\delta_{\sigma\sigma'}\gamma^{(2)}_{\sigma\sigma}(q')=\delta_{\sigma\sigma'}\sum_r e^{-iq'r}\sum_J V^{(n)2}G_\sigma(r)G_\sigma(r)\delta_{\boldsymbol{r},\boldsymbol{\delta}_J}, \quad \text{(A19)}$$

where $q'=(\boldsymbol{q},i(\epsilon_n+\epsilon_{n'}+\omega_m))$. We cannot approximate $\gamma^{(3,4)}_{\sigma\sigma}(\boldsymbol{k},\boldsymbol{k}';\boldsymbol{q})$ to be of a desired form and therefore simply neglect them. For $\gamma^{(5)}_{\sigma\sigma'}$, we put $\boldsymbol{R}=\boldsymbol{R}'$ and obtain

$$\gamma^{(5)}_{\sigma\sigma'}(k,k';q)=[\delta_{\sigma-\sigma'}U^2+W(\boldsymbol{q})]P_0(k-k'), \quad \text{(A20)}$$

where

$$W(\boldsymbol{q})=\frac{1}{N_{\rm L}}\sum_{\boldsymbol{k}}V(\boldsymbol{k}+\boldsymbol{q})V(\boldsymbol{k})=\sum_J V^{(n)2}\cos(\boldsymbol{q}\cdot\boldsymbol{\delta}_J). \quad \text{(A21)}$$

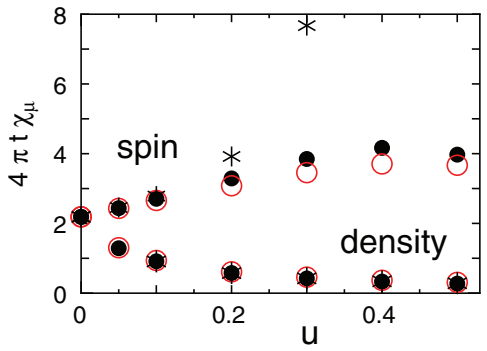

FIG. 15. (Color online) Compressibility and spin susceptibility as functions of interaction strength u. Black symbols represent results obtained from single-particle Green's function, and red symbols those obtained from response functions. Stars stand for results without contributions from vertex corrections.

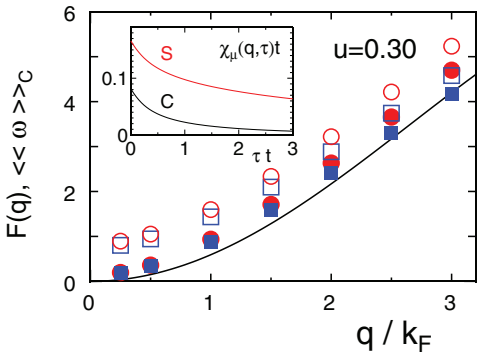

FIG. 16. (Color online) Check of the f-sum rule: Solid line stands for $F(\boldsymbol{q})$ defined by Eq. (39), and closed symbols represent the first moment of the dynamic structure factor $C(\boldsymbol{q},\omega)$. Open symbols stand for the results without contributions from vertex corrections. Dots and squares represent results obtained with different fitting methods (see text). The inset shows $\chi_\mu(\boldsymbol{q},\tau)$ at $q = 0.25k_{\rm F}$ for small τ.

No approximation is made for terms proportional to U^2. Finally, for $\gamma^{(6)}_{\sigma\sigma'}$, we put $\boldsymbol{R} = -\boldsymbol{R}'$ and find

$$\gamma^{(6)}_{\sigma\sigma'}(k,k';q) = -[\delta_{\sigma-\sigma}U^2 + W(\boldsymbol{q})]K_0(k+k'+q). \quad \text{(A22)}$$

Again, no approximation is made for the term proportional to U^2.

Finally, we obtain

$$\begin{aligned}\gamma_{\rm c}(k,k;q) &= \gamma_{\uparrow\uparrow}(k,k';q) + \gamma_{\uparrow\downarrow}(k,k';q)\\ &= [2U^2 + 2UV(\boldsymbol{k}-\boldsymbol{k}') + V(\boldsymbol{k}-\boldsymbol{k}')^2\\ &\quad + 2W(\boldsymbol{q})]P_0(k-k') - [U^2 + 2W(\boldsymbol{q})]\\ &\quad \times K_0(k+k'+q) + \gamma^{(2)}(q') \qquad \text{(A23)}\end{aligned}$$

and

$$\begin{aligned}\gamma_{\rm s}(k,k';q) &= \gamma_{\uparrow\uparrow}(k,k';q) - \gamma_{\uparrow\downarrow}(k,k';q)\\ &= [2UV(\boldsymbol{k}-\boldsymbol{k}') + V(\boldsymbol{k}-\boldsymbol{k}')^2]P_0(k-k')\\ &\quad + U^2K_0(k+k'+q) + \gamma^{(2)}(q'). \qquad \text{(A24)}\end{aligned}$$

To assess the validity of the approximation made for vertex corrections, we have checked the compressibility sum rule and f-sum rule. Figure 15 shows the compressibility and uniform spin susceptibility. We can obtain these quantities by calculating the single-particle Green's function. We can also calculate them as a static limit of response functions. Both results must agree in the conserving approximation, but as we have made approximations for the vertex corrections, the agreement will not be perfect. Figure 15 shows that the agreement is almost perfect for the density response function. Actually, for the compressibility, the effect of vertex corrections is insignificant. For the spin response function, slight disagreement is found, but the vertex corrections significantly improve the agreement. Indeed, without the vertex corrections, the uniform susceptibility diverges at $u \gtrsim 0.3$. The spin susceptibility is found to decrease at $u \gtrsim 0.4$. This is an artifact of the second-order perturbation theory. The SCSOPT tends to underestimate the spin susceptibility (in the dilute Hubbard model), and the calculated spin susceptibility decreases for large u in contrast to the exact results.[20]

We have also checked the f-sum rule. Figure 16 compares $F(\boldsymbol{q})$ defined by Eq. (39) and $\langle\langle\omega\rangle\rangle_{\rm C} = -\partial\chi_{\rm C}(\boldsymbol{q},\tau)/\partial\tau|_{\tau=0}$ at $u = 0.30$. They must agree if the approximation is conserving. In fact, the value of the derivative at $\tau = 0$ depends on how it is calculated numerically. In Fig. 16, we show two results obtained in different ways. One is obtained using the two points at $\tau = 0$ and β/M (squares), which gives the lowest bound of the first moment. The other is obtained by fitting a cubic curve to the five points at $\tau = i\beta/M$ ($i = 0$ to 4) (dots). We find that $\langle\langle\omega\rangle\rangle_{\rm C} \simeq \langle\langle\omega\rangle\rangle_{\rm S}$, if the method of fitting is the same. Therefore, in Fig. 16, we show only the first moment of $C(\boldsymbol{q},\omega)$. We see that $\langle\langle\omega\rangle\rangle_{\rm C}$ is slightly larger than $F(\boldsymbol{q})$ although the vertex correction significantly improves the degree of agreement. As $F(\boldsymbol{q})$ is vanishing as $q \to 0$, the deviation becomes relatively larger in the long-wavelength region.

[1]H. Godfrin, M. Meschke, M.-J. Lauter, H. M. Böhm, E. Krotscheck, and M. Panholzer, J. Low Temp. Phys. **158**, 147 (2010).
[2]H. Godfrin, M. Meschke, M.-J. Lauter, A. Sultan, H. M. Böhm, E. Krotscheck, and M. Panholzer, Nature (London) **483**, 576 (2012).
[3]C. H. Aldrich III and D. Pines, J. Low Temp. Phys. **32**, 689 (1978).
[4]D. W. Hess and D. Pines, J. Low Temp. Phys. **72**, 247 (1988).
[5]H. R. Glyde, B. Fåk, N. H. van Dijk, H. Godfrin, K. Guckelsberger, and R. Scherm, Phys. Rev. B **61**, 1421 (2000).
[6]E. Krotscheck, Phys. Rev. A **26**, 3536 (1982).
[7]H. M. Böhm, E. Krotscheck, M. Panholzer, H. Godfrin, H. J. Lauter, and M. Meschke, J. Low Temp. Phys. **158**, 194 (2010).
[8]H. M. Böhm, R. Holler, E. Krotscheck, and M. Panholzer, Phys. Rev. B **82**, 224505 (2010).
[9]M. Panholzer, H. M. Böhm, R. Holler, and E. Krotscheck, J. Low Temp. Phys. **158**, 135 (2010).
[10]R. Hobbiger, R. Holler, E. Krotscheck, and M. Panholzer, J. Low Temp. Phys. **169**, 350 (2012).
[11]H. R. Glyde and S. I. Hernadi, Phys. Rev. B **28**, 141 (1983).
[12]H. R. Glyde and S. I. Hernadi, Phys. Rev. B **29**, 4926 (1984).

[13]B. Tanatar, E. F. Talbot, and H. R. Glyde, Phys. Rev. B **36**, 8376 (1987).
[14]B. E. Clements, C. W. Greeff, and H. R. Glyde, Phys. Rev. B **44**, 5216 (1991).
[15]H. Takahashi and D. S. Hirashima, J. Low Temp. Phys. **121**, 1 (2000).
[16]Usually, in the RPA, exchange terms are neglected. In this paper, we call the approximation where the vertex corrections for response functions are neglected the RPA. In this approximation, the exchange terms are also considered.
[17]A. Kotani and D. Hirashima, J. Phys.: Conf. Ser. **400**, 012035 (2012).
[18]C. P. Lusher, B. P. Cowan, and J. Saunders, Phys. Rev. Lett. **67**, 2497 (1991).
[19]Effect of vertex corrections on spin fluctuations is essential in contrast to the case with charge fluctuations. Without vertex corrections, the spin susceptibility would diverge at $u \simeq 0.3$. See Appendix.
[20]H. Takahashi, J. Phys. Soc. Jpn. **68**, 3816 (1999).
[21]P. Nozières, J. Low Temp. Phys. **137**, 45 (2004).
[22]J. Boronot, J. Casulleras, V. Grau, E. Krotscheck, and J. Springer, Phys. Rev. Lett. **91**, 085302 (2003).
[23]For example, G. F. Giuliani and G. Vignale, *Quantum Theory of the Electron Liquid* (Cambridge University Press, Cambridge, 2005).
[24]A. Sultan, M. Meschke, H.-J. Lauter, and H. Godfrin, J. Low Temp. Phys. **169**, 367 (2012).
[25]K. Sköld, C. A. Pelizzari, R. Kleb, and G. E. Ostrowski, Phys. Rev. Lett. **37**, 842 (1976).